Energy & Environmental Science

Migration-assisted, Moisture Gradient Process for Ultrafast, Continuous CO2 Capture from Dilute Sources at Ambient Conditions

Journal:	*Energy & Environmental Science*
Manuscript ID	EE-ART-09-2021-003018.R2
Article Type:	Paper
Date Submitted by the Author:	17-Dec-2021
Complete List of Authors:	Prajapati, Aditya; University of Illinois at Chicago, Chemical Engineering Sartape, Rohan; University of Illinois at Chicago, Chemical Engineering Rojas Solorzano, Tomas; Argonne National Laboratory Dandu, Naveen; Argonne National Laboratory Dhakal, Pratik; Oklahoma State University System, Chemical Engineering Thorat, Amey; Oklahoma State University System, Chemical Engineering Xie, Jiahan; Braskem America Inc Bessa, Ivan; Braskem SA Galante, Miguel; Braskem SA Andrade, Marcio; Braskem SA Somich, Robert; Braskem America Inc Reboucas, Marcio; Braskem SA Hutras, Gus; Braskem America Inc Diniz, Nathalia; Braskem SA Ngo, Anh; Argonne National Laboratory Shah, Jindal; Oklahoma State University System, Chemical Engineering Singh, Meenesh; University of Illinois at Chicago, Chemical Engineering

Migration-assisted, Moisture Gradient Process for Ultrafast, Continuous CO_2 Capture from Dilute Sources at Ambient Conditions

Aditya Prajapati[1], Rohan Sartape[1], Tomás Rojas[2], Naveen K. Dandu[2], Pratik Dhakal[3], Amey S. Thorat[3] ,Jiahan Xie[4], Ivan Bessa[5], Miguel T. Galante[5], Marcio H. S. Andrade[5], Robert T. Somich[4], Marcio V. Reboucas[5], Gus T. Hutras[4], Nathalia Diniz[5], Anh T. Ngo[1, 2], Jindal Shah[3], Meenesh R. Singh[1*]

[1] Department of Chemical Engineering, University of Illinois at Chicago, 929 W. Taylor St., Chicago, Illinois, USA 60607

[2] Material Sciences Division, Argonne National Laboratory, 9700 S Class Ave, Lemont, Illinois, USA 60439

[3] Department of Chemical Engineering, Oklahoma State University, 420 Engineering North, Stillwater, Oklahoma, USA 74078

[4]Braskem America Inc., 550 Technology Drive, Pittsburgh, PA, 15219

[5]Braskem S.A, Rua Eteno S/N, Camaçari, Bahia, Brazil

Corresponding Author

Prof. Meenesh R. Singh
Assistant Professor
Department of Chemical Engineering
929 W. Taylor St.
University of Illinois at Chicago
Chicago, IL 60607
Tel: (312) 996-3424
Email: mrsingh@uic.edu

Keywords: Continuous CO_2 Capture, Electrodialysis, Moisture Gradient, Flue gas, Carbon Capture and Sequestration

Broader context

The development of efficient CO_2 capture systems has received increasing attention due to the ever-increasing anthropogenic CO_2 concentration in the atmosphere. Current state-of-the-art technologies rely on energy-intensive pressure or temperature swing for CO_2 sorption from a point source like flue gas and regenerate the sorbents through similar energy-consuming processes. Moreover, these processes require process integration of capture and regeneration units for continuous operation. The massive energy penalties for a modest CO_2 capture flux are the bottleneck of scaling up such processes. Here we report an ultrafast CO_2 capture process driven by moisture gradient and electric field with low energy consumption. This is a modular process powered by renewable energy to capture CO_2 from the air or the flue gas.

Abstract:

The current industrially relevant CO_2 capture technologies require high operating and capital costs or are energy-intensive, rendering them inefficient and unsustainable for long-term use. The higher operating cost is primarily due to the energy-intense swing of pH- or temperature-dependent equilibrium of CO_3^{2-} and HCO_3^- to capture CO_2. CO_2 can be captured in an aqueous solution with OH^- to convert it into HCO_3^-, which can be turned back into CO_3^{2-} and CO_2 using either temperature or pH swing. This captured CO_2 can be either sequestered or chemically transformed into a usable product. The challenges with this technology are the limited carbon capacity of the aqueous solvent system, higher energy requirement for solvent regeneration, and loss of solvent through evaporation. The water-dependent equilibrium of CO_2 with CO_3^{2-} and HCO_3^- can be a cost-effective alternative to the existing technologies. Here, we exploit this phenomenon by establishing a water gradient across an anion exchange membrane that separates organic solvent saturated with OH^- and an aqueous solution. The organic solution contains ethylene glycol saturated with KOH that captures CO_2 for dilute sources such as air or flue gas and produces a high concentration of HCO_3^- that migrates towards the aqueous side, where HCO_3^- converts back to CO_2 for its end-use. The current efficiency of CO_2 capture is nearly 100%, with a tunable flux CO_2 capture flux that is controlled by the applied current density. The water-dependent CO_2 capture and release kinetics are measured using in situ Fourier-transform infrared spectroscopy and validated using density functional theory. A detailed transport model confirms the CO_2 capture, transport, and release mechanism for varying water concentration in the organic solution, membrane thickness, and the applied current. Machine learning model predicts the performance curve for this process that relates CO_2 saturation in aqueous solution to the CO_2 capture efficiency, humidity of flue gas, and current density. The validated prototype of the electrodialysis system showed an unprecedented CO_2 capture flux of 2.3 mmol/m^{2}s, which is 100 times higher than the state-of-the-art existing CO_2 capture technologies. The technoeconomic analysis predicts ~\$145/ton of CO_2 for 1000 ton/hr of CO_2 capture capacity.

1 Introduction

The anthropogenic emissions contribute ~37.1Gt of CO_2 in the atmosphere and raise the CO_2 concentrations by 1.6 ppm annually (1, 2). Consequently, the melting of ice caps, rising sea levels, and ocean acidification are some of the significant effects of global warming. These factors pose a severe threat to the earth's climate, and therefore, there is an urgent need to develop technologies to abate this rise in the CO_2 concentration in the atmosphere. In this framework, several thermochemical (3-5), electrochemical (6-8), and biochemical (6, 9) CO_2 capture technologies have been explored. CO_2 capture from sources such as fossil-fuel-based power plants and coal-based chemical processes is commonly practiced using pre-combustion, oxy-fuel combustion, and post-combustion CO_2 capture techniques (2). Pre-combustion CO_2 capture is prevalent in integrated gasification combined cycle (IGCC) plants where the resultant pressurized gas minimizes the emission of impurities such as SO_x and NO_x during the power generation cycle (10, 11). In the oxy-fuel technique, the use of pure oxygen for fuel combustion eliminates SO_x and NO_x emissions and produces a CO_2-rich flue gas stream. However, the requirement of pure oxygen offsets this advantage (12, 13). Pre-combustion and oxy-fuel combustion CO_2 capture technologies require a significant investment to integrate these processes in a pre-existing power plant. Post-combustion CO_2 capture is particularly attractive due to the availability of a broad range of technologies that can be retrofitted to any conventional coal or gas-fired power plants or even in the industries with significant CO_2 exhausts (14). Numerous CO_2 capture techniques have been explored as post-combustion CO_2 capture technologies, such as liquid absorption, cryogenic distillation, adsorption, and membrane separation (15, 16). A conventional Rectisol wash technology using methanol-based physical absorption of CO_2 is deployed in many ammonia plants. Operating the CO_2 capture unit at low temperature and high pressure enhances the solubility of CO_2 in methanol but also increases the energy intensity of this process (17). Liquid absorbents such as monoethanolamine (MEA), diethanolamine, and aqueous hydroxide solutions are widely employed in industry to capture CO_2 selectively by chemical absorption (15, 18). The amine-based processes suffer from solvent losses due to evaporation and high viscosity upon CO_2 absorption. The strong binding of CO_2 with the amine functionality necessitates high temperatures to release the captured CO_2 and regenerate the solvent (19), which negatively impacts the energy efficiency of the process. In the case of aqueous hydroxide solutions, the conversion of HCO_3^- to CO_3^{2-} limits the CO_2 capture capacity and results in high energy consumption for releasing CO_2. Another concern is water loss during the causticization-calcination process for regenerating $Ca(OH)_2$ for the hydroxide-based approaches. Solid adsorbents like metal-organic frameworks (MOFs)(20), CaO(1), and alkali metal CO_3^{2-}(20, 21) exhibit >85% adsorption efficiency(15) and are also attractive candidates for CO_2 capture. However, regenerating these sorbents is an energy-intensive process. In a single-pass operation, the membrane separation technology captures CO_2 from a mixture of gases in the feed by size exclusion or relative electrostatic attraction (22-24).With the development of durable membranes and pumping of CO_2 being the only major operating cost, there is a promising outlook on the large-scale implementations for CO_2 capture using membrane technology. However, while capturing CO_2 from dilute sources such as flue gas and air, large volumes of gases need to be processed for CO_2 capture and membrane regeneration (25-27).

Insofar, the present state-of-the-art CO_2 capture technologies using MEA, solid sorbents, and membranes have shown promising scale-up capabilities. However, they have a moderate to high energy requirement for capturing the CO_2, and since the regeneration of the CO_2 capture media is done by temperature or pressure swings, they also have a high energy penalty of regeneration. Moreover, this regeneration makes the processes discontinuous as no CO_2 can be captured during this regeneration step. Process modifications using auxiliary regeneration units like chemical looping and multiple fluidized bed adsorbers have attempted to circumvent this challenge but only at the expense of higher energy consumption.(15, 20) At present, even the most efficient CO_2 capture processes have shown CO_2 capture flux only in the order of 10^{-3}–10^{-4} mmol of $CO_2/m^2/s$(28, 29). Therefore, there is a need to incorporate a low-energy regeneration step into the CO_2 capture mechanism to make it continuous and more efficient without the need for auxiliary regeneration units to meet the 2050 global CO_2 mitigation milestone.

It is imperative to look at newer methods for CO_2 capture to realize the potential of making them continuous. Water-driven CO_2 capture techniques are in their infancy and are particularly attractive due to their low energy penalty (30-32). Hydrate-based CO_2 separation is a water-driven technology where CO_2 forms hydrate with water or water-miscible solvents under high pressure and can be separated from a feed with a mixture of gases. Another new technology developed by Lackner, Wang, and coworkers(32, 33), uses moisture swing to capture CO_2 directly from the air where a quaternary amine ion-exchange resin supported on a polymeric backbone acting as the anion-exchange membrane (AEM) that absorbs CO_2 in a water-deprived (dry or organic) environment in the form of HCO_3^- and CO_3^{2-} and releases it as CO_2 in a wet (aqueous) environment by virtue of the CO_3^{2-}-HCO_3^- equilibrium. This mechanism can be exploited by keeping a constant water-deprived environment on one side of the AEM with a continuous supply of CO_2 and an aqueous environment on the other side, thereby establishing a gradient of concentration of water across the AEM. The mechanism can be described by the following reactions:

Organic side (CO_2 capture)	$CO_2 + OH^- \rightleftharpoons HCO_3^-$	(1)
Aqueous side (CO_2 release)	$2HCO_3^- \rightleftharpoons CO_2 + H_2O + CO_3^{2-}$	(2)

In this work, we propose a novel carbon capture and release process that utilizes a CO_2 binding organic liquid (CO2BOL)(34)-a solution of KOH dissolved in ethylene glycol- to efficiently chemisorb CO_2 as HCO_3^-, an AEM to facilitate the transfer of these HCO_3^- ions, and an aqueous electrolyte, where water converts HCO_3^- to CO_2 and CO_3^{2-}. The HCO_3^- and CO_3^{2-} remain in equilibrium in this aqueous medium governed by the pH of the solution (16). The water-splitting reaction leading to oxygen evolution on the aqueous side acts as a source of H^+ ions that further combine with CO_3^{2-} to form CO_2 thereby preventing the accumulation of CO_3^{2-} on the aqueous side. This conversion of HCO_3^- to CO_2 and CO_3^{2-} is the CO_2 release process which is an integral part of this mechanism. It has no additional energy penalty which makes it an attractive mechanism to explore. To enhance the rate of this process, an electric field is established to migrate HCO_3^- from the CO2BOL across AEM to the aqueous electrolyte. The schematic and the mechanism of this migration-assisted moisture-gradient (MAMG) CO_2 capture process are shown in Figure 1. These processes are implemented in an electrochemical cell where the CO2BOL (CO_2 capturing

solution) and aqueous electrolyte (CO_2 releasing solution) are separated by AEM, as seen in Figure 1A. The scope of this study involves an experimental determination of water-driven kinetics of the CO_3^{2-}-HCO_3^-- equilibrium in a water-deprived environment responsible for the moisture-gradient CO_2 capture; CO_2 capture kinetics using CO2BOL; and computational design and evaluation of the MAMG process with the experimentally determined kinetic and equilibrium parameters using COMSOL Multiphysics. We also describe the incorporation of data-driven approaches such as machine learning (ML) with the physics-based COMSOL computational model to aid in identifying optimum operating conditions and accelerate the design and development of the MAMG process. Finally, a techno-economic analysis is conducted to assess the feasibility of deploying MAMG on a commercial scale.

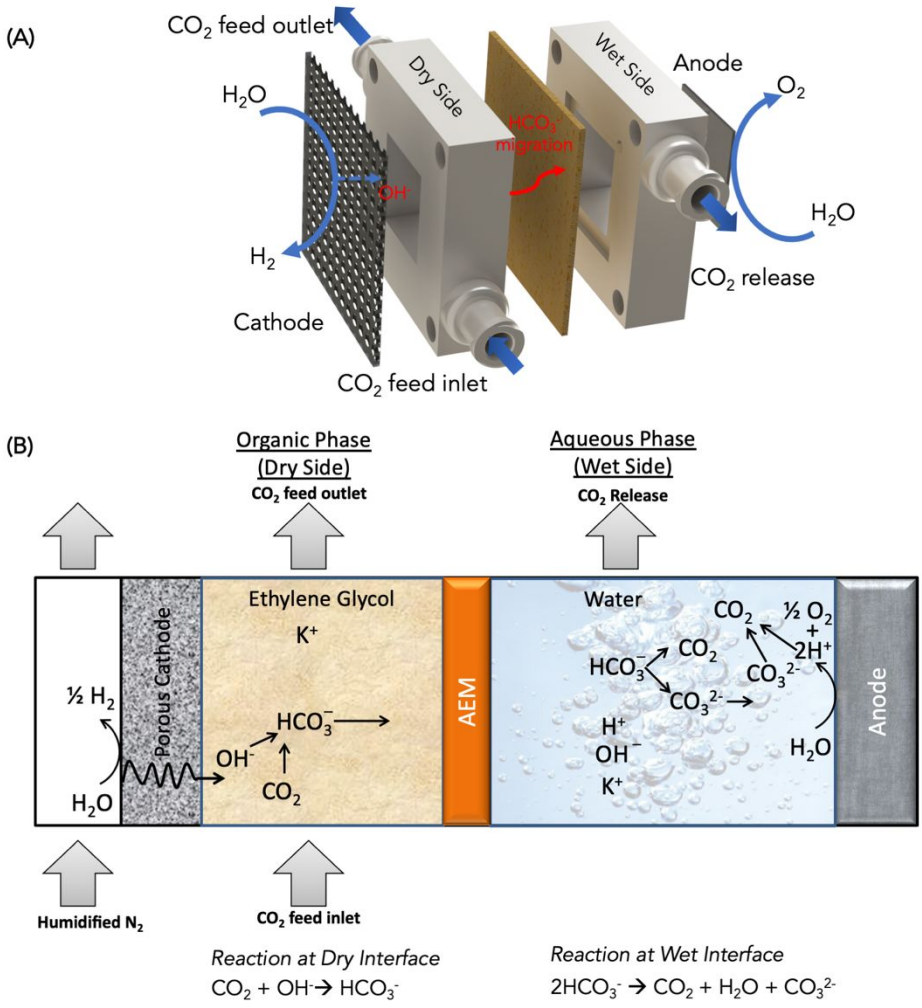

Figure 1: (A) Schematic diagram of the electrochemical cell setup for the MAMG CO_2 capture system. (B) Mechanism of CO_2 capture. The green represents the organic (dry) side, and the blue represents the aqueous (wet) side of an AEM.

The rest of the article is organized as follows- The Methods and Materials section describes the Fourier transform infrared spectroscopy (FTIR) and Karl Fischer (KF) titrations to determine

the water-driven kinetics of the CO_3^{2-}-HCO_3^-- equilibrium, the experimental setup for CO_2 capture experiments using CO2BOL, density functional theory (DFT) predicted reaction energy of HCO_3^- going to CO_3^{2-} and CO_2 in a water-deprived environment, and the setup of a 1D simulation of the MAMG CO_2 capture system using COMSOL Multiphysics, and the development of ML models for accelerated identification of optimum operating conditions. Results and Discussion section describes the in-situ FTIR analysis of the water-driven kinetics of the CO_3^{2-}-HCO_3^- equilibrium supported by the DFT predicted reaction energies, the CO_2 capture kinetics, computational evaluation of the performance of the CO_2 capture system by studying the effect of migration current, membrane width, and the concentration of water on the water-deprived side of the membrane. It also includes the ML models' insights describing the importance of process parameters of the MAMG CO_2 capture process and the techno-economic analysis to assess the feasibility of scaling up such a process. Conclusion and Perspectives section presents the conclusions and strategies to implement an efficient moisture-gradient CO_2 capture.

2 Methods and Materials

2.1 Experimental Methods

2.1.1 Fourier Transform Infrared (FTIR) spectroscopy

FTIR spectroscopy was performed to quantify the concentration of CO_3^{2-} and HCO_3^- for varying H_2O concentration in a non-aqueous solvent (CH_3OH) to understand the water-dependent CO_3^{2-}-HCO_3^- equilibrium. The FTIR bench was a Bruker Invenio S with a Pike VeeMax II variable angle attenuated total reflectance (ATR) accessory and a 60^o Ge face-angled crystal. A mid-band liquid N_2 cooled MCT detector was used, and for each experiment, the spectra acquired were averaged over 1500 acquisitions at a resolution of 4 cm^{-1}. A custom-made 3D printed cell of a maximum capacity of 4 ml was placed on top of the Ge crystal, where all the FTIR experiments were performed. The intensity of the HCO_3^- band at 1633 cm^{-1} and the CO_3^{2-} band at 1450 cm^{-1} were individually calibrated at different concentrations of HCO_3^- and CO_3^{2-} in CH_3OH.

2.1.2 Karl-Fisher (KF)titrations

KF titrations were performed to determine the total water content in the system containing the previously determined HCO_3^- and CO_3^{2-}. A custom-made 3D-printed cell of the same capacity as the cell used in the FTIR was used for this study. A solution of CH_3OH, $NaHCO_3$, and a known amount of H_2O in the cell was well mixed using a magnetic stirrer. Two Cu electrodes were placed on the opposite ends of the cell, and the cell's open circuit potential (OCP) was constantly monitored. 20 µl of KF titrant was added to the cell periodically, and the endpoint was detected by a sharp increase in the OCP of the cell. This endpoint is an indicator of the total H_2O in the solution. Therefore, the combination of FTIR and KF titrations can provide HCO_3^-, CO_3^{2-} and H_2O concentration, and the equilibrium constant for $2HCO_3^- \rightarrow CO_2 + CO_3^{2-} + H_2O$ can be calculated using the equation below:

$$K = \frac{[CO_2][CO_3^{2-}][H_2O]}{[HCO_3^-]^2} \approx \frac{[CO_3^{2-}]^2[H_2O]}{[HCO_3^-]^2} \quad (3)$$

Here, we consider $[CO_2] \approx [CO_3^{2-}]$ because of the reaction stoichiometry and because the CO_2 released is below the solubility limit of the aqueous side and no gaseous CO_2 is evolved during the CO_2 release process.

2.1.3 Rate of HCO_3^- formation on the organic side

CO_2 was sparged into the organic solution of 1.2M KOH dissolved in a CO2BOL to observe the rate of HCO_3^- formation as seen in eq.(1). The concentration of the HCO_3^- formed was monitored by observing the change in resistance of the solution using electrochemical impedance spectroscopy (EIS) on a Biologic SP-300 potentiostat. Initially, a calibration curve was obtained by dissolving various concentration ratios of HCO_3^- and OH^- in the CO2BOL using the solution resistance, which was correlated to the HCO_3^- concentration to determine the flux of CO_2 chemisorbed as HCO_3^-.

2.1.4 Migration-assisted moisture-gradient (MAMG) CO_2 capture

The MAMG CO_2 capture experiments were done to determine the flux of CO_2 capture. A custom 3D printed electrochemical cell (Figure 1A) was used with carbon paper electrodes of 20x20 mm (Area: 4 cm^2).The organic side was a 1.2M KOH dissolved in CO2BOL sparged with 10% CO_2 and balance N_2, the aqueous side was 0.1M KOH pre-equilibrated with CO_2 in water at a pH of 7.8, and both separated by a Snowpure Excellion AEM. A DC source was used to drive the migration in constant current mode with a current of 25 mA. The change in the pH of the aqueous side was used to determine the flux of CO_2 captured. All the MAMG CO_2 capture experiments were performed at room temperature (25^{o}C).

CH_3OH is used as a CO2BOL for the FTIR and KF titration experiments instead of EG only because of the ease of subtraction of the background FTIR spectra of CH_3OH compared to EG and the primary solvent of the KF titrant being CH_3OH. Using CH_3OH allowed for a more precise estimation of water-dependent reactions responsible for MAMG CO_2 capture without the interference of EG. A detailed description of the experimental methods is given in section S1 of the ESI.

2.2 Computational Methods

2.2.1 DFT predicted reaction energy

To determine the ΔG of equation (2) in a solvent, DFT calculations were performed using B3LYP(35-37) functional with 6-31+G(2df,p) basis set utilizing Gaussian09 software code.(38) For performing calculations in the presence of a solvent, we used the Polarizable Continuum Model (PCM)(39) by specifying the static (or zero-frequency) dielectric constant (ϵ) of the solvent mixture (water +EG) at different concentrations. With each volume of water added, we obtained a different value of ϵusing the formulation developed by Jouyban and Soltanpour(40). In this methodology, the $\epsilon$of a solution is calculated based on the individual $\epsilon$of the solvents as well as their Abraham solvation parameters. At each of the ϵ values, DFT optimization and solvent calculation of the reactants and products were performed and Gibbs free energies of each of the

species were used to calculate ΔG of the reaction. The estimated ϵ of the solution with EG and different concentrations of water and ΔG calculations are given in section S2.1 of the ESI

2.2.2 Multiphysics model

A one-dimensional model for the MAMG CO_2 capture system was developed using COMSOL Multiphysics to solve the Nernst-Planck equation for the transport of different ionic species using models designed for an electrochemical cell for CO_2 reduction previously developed by Singh et al. (41, 42). A time-dependent analysis was done to see the development of concentration profiles of the species in the membrane. The CO_3^{2-}-HCO_3^- equilibrium reactions were set to be water-dependent that were obtained as a result of the FTIR and KF titration experiments, and the organic side was modeled as a well-mixed electrolyte with high diffusion coefficients for all the species. The rate of HCO_3^- formation and the migration current were also taken from the experiment to emulate the experimental conditions closely and were implemented in the simulation as follows:

Rate of HCO_3^- formation: On the organic side, CO_2 is constantly sparged into the system, which also acts as a source of HCO_3^-. This source term is the experimentally obtained rate which is modeled as:

$$N_{HCO_3^-} = \frac{d[HCO_3^-]}{dt} \quad (4)$$

where $N_{HCO_3^-}$ is the flux determined from the experiments.

Migration current: The migration current is a parameter chosen from the experiments and is implemented on the anodic side in the model as:

$$-\boldsymbol{n} \cdot \boldsymbol{i} = i_0 \quad (5)$$

where $\boldsymbol{i}$ is the current density vector and $\boldsymbol{i}$of CO_2 utilization, $-\boldsymbol{n}$ is the normal vector pointing inward, and $i_0$is the migration current value from the experiments.

2.2.3 Machine learning models

This study investigated two different ML algorithms to rapidly identify optimum operating conditions for a MAMG CO_2 capture system - Multiple Linear Regression (MLR) and neural network (NN). The models were developed on 126 data points, with 80% of the data used as a training set and the remaining 20% was used as a test set. A set of 20 random trials were carried out to evaluate the performance of the model algorithms to avoid any biases that may arise due to splits.

A detailed description of the computational methods can be found in section S2 and S6 of the ESI.

3 Results and Discussion

The experimental determination of the water-dependent CO_3^{2-}-HCO_3^- equilibrium supported by a DFT predicted equilibrium reaction energies is discussed next. This section also encompasses the results evaluating the continuum model and the performance of the CO_2 capture technique with different process parameters like migration current, AEM width, and relative humidity of the CO_2 feed.

3.1 Water-dependent reaction

The key reaction that drives this process can be seen in eq. (2) where H_2O autocatalyzes this reaction. This autocatalytic reaction can be realized by simply adding water to baking soda that causes CO_2 effervescence. This is a well-known equilibrium reaction, which has not been investigated thoroughly for its dependence on H_2O. Following plausible reaction mechanism can represent this autocatalytic HCO_3^- decomposition.

$$\begin{aligned} HCO_3^- + H_2O &\rightleftharpoons CO_3^{2-} + H_3O^+ \\ HCO_3^- + H_3O^+ &\rightleftharpoons CO_2 + 2H_2O \end{aligned} \qquad (6)$$

FTIR spectroscopy was performed to identify the relationship between the concentration of CO_3^{2-} and HCO_3^- for varying H_2O concentrations in CH_3OH solvent. CH_3OH was chosen as a solvent to retain the HCO_3^- in their pure form and prevent them from equilibrating with CO_3^{2-} as seen in an aqueous system. HCO_3^- were calibrated by relating the known concentration of $NaHCO_3$ dissolved in CH_3OH to the intensity at 1633 cm^{-1}. Similarly, the CO_3^{2-} were calibrated by observing the change in the intensity at 1450 cm^{-1}. Figure 2A shows the FTIR spectra used to study the equilibrium reaction. A known amount of NaOH was dissolved in CH_3OH, and CO_2 was sparged into the system, resulting in the conversion of OH^- to HCO_3^-. The concentration of HCO_3^- was determined using the previously established calibration curve seen in section S1 of the ESI. 2 ml of H_2O was added to this solution, and the spectra were recorded to quantify CO_3^{2-} formed via HCO_3^- decomposition. The same experiment was repeated with increasing quantities of H_2O to quantify the H_2O-dependent equilibrium constant. As can be seen from Figure 2A, there are no HCO_3^- stretches in CH_3OH and NaOH solution. When the CO_2 sparging starts, HCO_3^- stretches start appearing at 1633 $cm^{-1,}$ indicating the formation of HCO_3^-. As the water is added to the system, the CO_3^{2-} stretches at 1450 cm^{-1} become more intense, confirming the influence of water in this equilibrium. The spectra between 1300 and 1700 cm^{-1} can be seen in Figure S3 of the ESI. Since the equilibrium of HCO_3^- decomposition reaction also produces H_2O when the reaction shifts from HCO_3^- to CO_3^{2-}, the quantity of H_2O in the solution is larger than the quantity added. This extra H_2O is quantified by Karl-Fisher (KF) Titrations, and the equilibrium constant K was determined by eq. (3). Figure 2B shows the dependence of K on the concentration of water. As the water concentration increases, the value of K approaches the value close to that of the well-defined CO_3^{2-}-HCO_3^- equilibrium in an aqueous solution. (41, 43) This is further supported by the trend in the DFT predicted Gibbs free energy (ΔG) in Figure 2C. The reaction energies for eq. (2) show positive values at lower concentrations of water thereby implying the conversion of HCO_3^- to CO_3^{2-} and CO_2 is more challenging in such an environment. The ΔG becomes negative after the

concentration of water reaches 3M suggesting the spontaneity of the reaction at higher water concentrations.

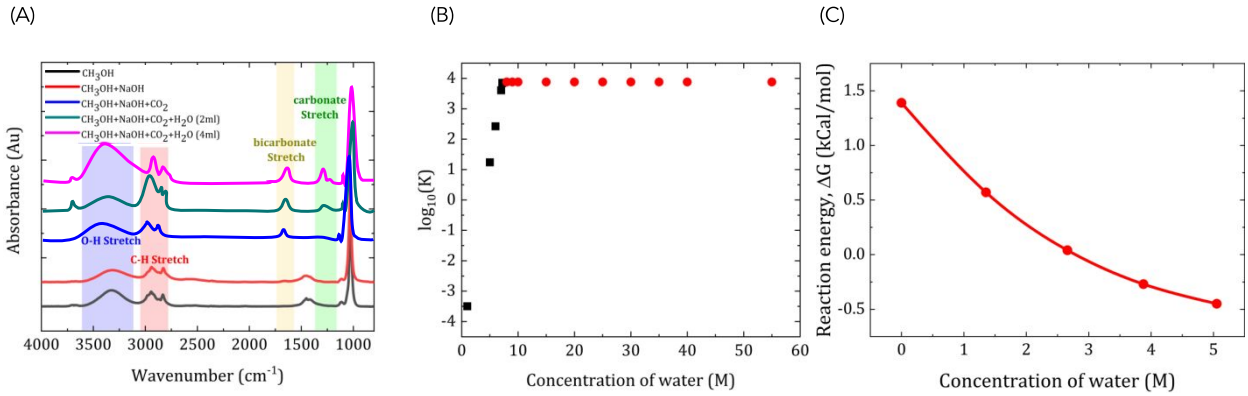

Figure 2: (A) FTIR spectra of pure CH_3OH (black), CH_3OH and NaOH (red), CH_3OH and NaOH with CO_2 sparged (blue), CH_3OH and NaOH with CO_2 sparged and added water (2ml-teal, 4ml-magenta). (B) Change of the water-dependent equilibrium constant as a function of water. The black squares show the experimental values from this work approaching the equilibrium constant (red circles) value in the aqueous solution. (C) DFT predicted reaction energy of eq. (2) in the presence of different concentrations of water.

3.2 Kinetics of CO_2 capture on the organic side

CO_2 is chemisorbed in the 1.2M KOH solution in CO2BOL to form HCO_3^- by eq. (1). To determine the amount of OH^- converted to HCO_3^-, a calibration of solution resistance vs. HCO_3^- concentration is initially established, as seen in Figure 3A. As the K^+ is just a spectator ion being common to both KOH and $KHCO_3$, the calibration is independent of K^+ and is dependent exclusively on the concentration of OH^- and HCO_3^-. Since OH^- has higher ionic mobility than HCO_3^-, the solution resistance increases with HCO_3^- concentration (and the consequent decrease in the OH^- concentration).

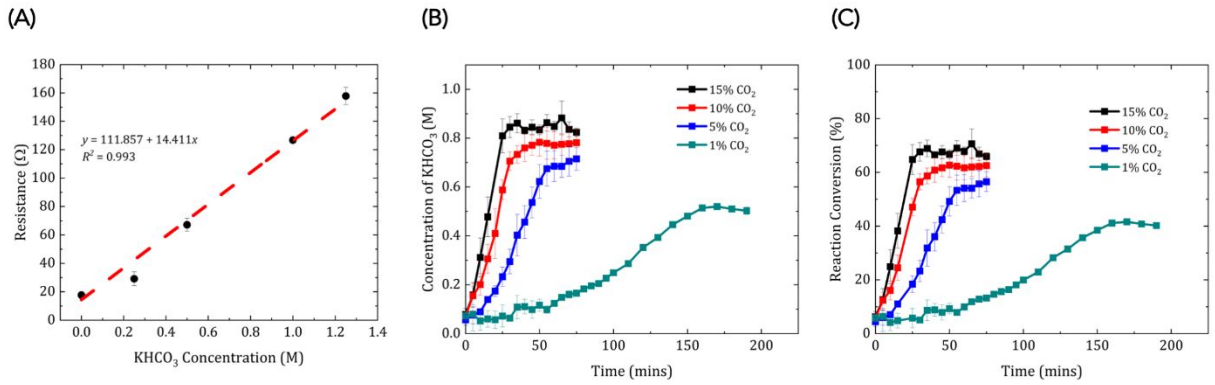

Figure 3: (A) Calibration curve for the solution resistance of varying concentrations of HCO_3^- in CO2BOL. (B) and (C) Kinetics of CO_2 capture in CO2BOL with varying feed concentration of CO_2 showing (B) the increase in HCO_3^- concentration and (C) the overall reaction conversion.

The kinetics of CO_2 capture on the organic side for varying concentrations of CO_2 can be realized in Figure 3B. CO_2 was sparged into the organic side, and the dynamic change in the solution resistance was correlated to the HCO_3^- concentration using the calibration from Figure 3A. The concentration of CO_2 increases linearly with time and then reaches a plateau. The time to reach the plateau and the concentration at the plateau are proportionally dependent on the concentration of CO_2 in the feed. This is because, at higher concentrations, the mass transfer gradient from the feed to the CO2BOL is higher, which leads to faster kinetics. Moreover, not all the OH^- is converted to HCO_3^- as this process of simple chemisorption is thermodynamically limited by the partial pressure of the CO_2 in the feed following Henry's law. (41) This constant CO_2 feed in the organic side can be expressed as:

$$R_{CO_2} = kaK_0(C_{CO_{2,feed}} - C_{CO_{2,CO2BOL}}) \quad (7)$$

where R_{CO_2} is the feed rate of CO_2, ka is the mass transfer coefficient, K_0 is the Henry's constant, $C_{CO_{2,feed}}$ is the concentration of CO_2 in the feed, and $C_{CO_{2,CO2BOL}}$ is the concentration of CO_2 in the CO2BOL. The slopes in Figure 3B indicate the rate of formation of HCO_3^- which is used as a source term for HCO_3^- in the continuum model using eq. (4).

3.3 Effect of process parameters on CO_2 capture

The migration was implemented to continuously capture CO_2 on the organic side and transport the captured CO_2 to the aqueous side. The Multiphysics model was benchmarked from the results obtained from the experiments at a migration current (i_m) of 25 mA, feed relative humidity (RH) 0 %, and membrane thickness 100 μm as seen in Figure 4A. The model closely follows the change in pH observed in the experiment. pH is used as the parameter to measure the concentration of CO_2 on the aqueous side. A detailed calculation for the conversion from pH to $[CO_2]$ can be seen in section S3 of the ESI.

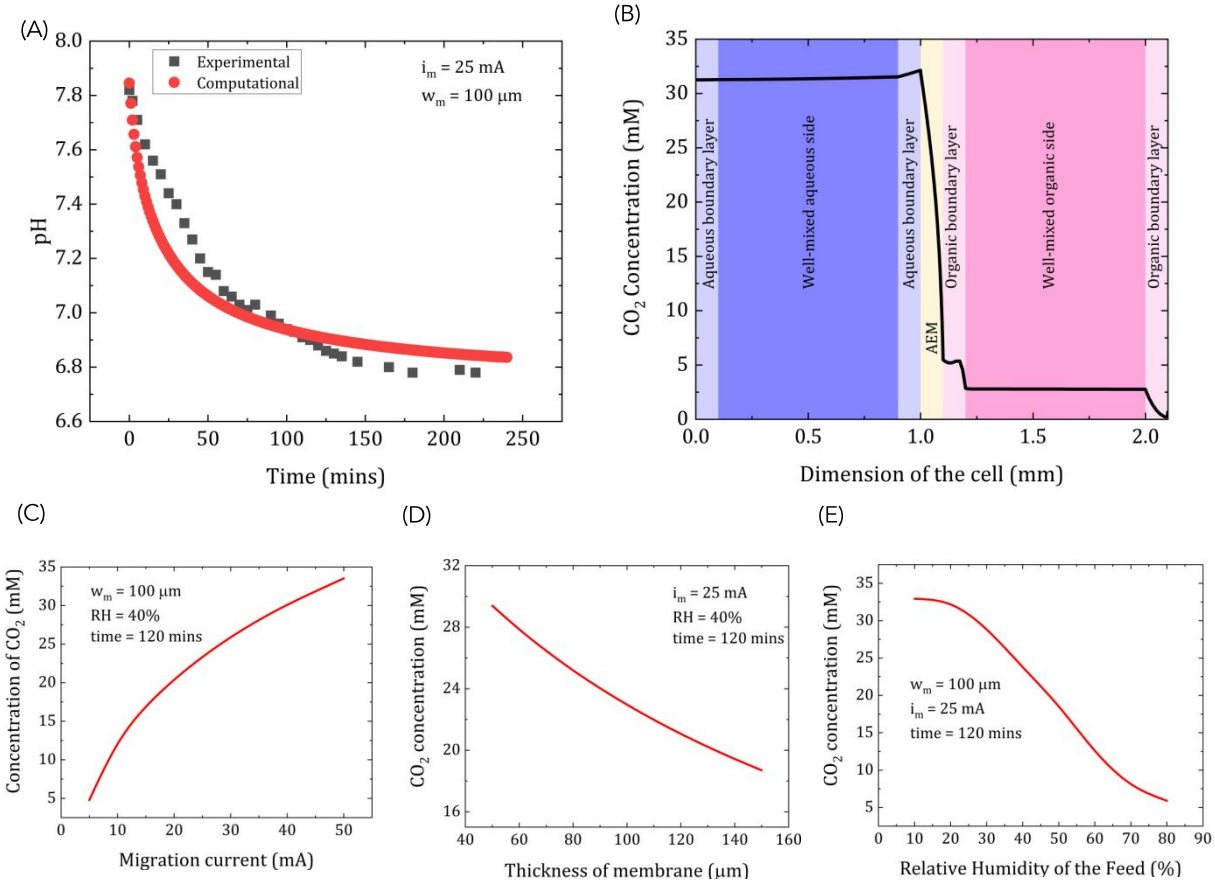

Figure 4: (A) Comparison of the change in pH in the experimental vs. continuum model for MAMG CO_2 capture. (B) Steady state CO_2 concentration profile across the electrochemical cell. Effect of (C) migration current, (D) membrane thickness, and (E) relative humidity of feed in the MAMG CO_2 capture system.

The drop in the pH indicates the HCO_3^- ions are migrating across the AEM and are immediately in equilibrium with CO_2 and CO_3^{2-} thereby lowering the pH of the KOH solution on the aqueous side. The CO_2 capture process shows a high average flux of 2.3 mmol of CO_2 captured/m^2/s at 75 mA of migration current, which is two orders of magnitude higher than any of the present state-of-the-art CO_2 capture processes. Figure 4B shows the concentration profile of CO_2 in the electrochemical cell. The CO_2 in the organic side is at a very low concentration as it is continuously reacting with the OH^- to form HCO_3^-. Across the AEM, a sharp gradient can be seen as the transported HCO_3^- ions are getting converted back to CO_2 and CO_3^{2-} due to the presence of a large concentration of water moving towards the aqueous side.

The computationally evaluated effect of processes parameters on CO_2 concentration at the aqueous side can be seen in Figure 4C-E. Since the CO_2 concentration reaches its solubility limit at a steady state, it is more appropriate to understand the effect of the process parameters under transient conditions. Therefore, all the effects considered here are measured at 120 mins when the CO_2 capture system has not reached a steady state. Figure 4C shows the effect of migration current varied from 5 to 50 mA. At low migration current densities, the driving force for the HCO_3^- ions

to move through the AEM is primarily due to the diffusional gradients. These gradients are necessary but not sufficient to facilitate a fast crossover of HCO_3^- and hence, the transient CO_2 concentration on the aqueous side is also lower at lower migration current densities. As we start reaching higher current densities, the CO_2 concentration starts reaching its solubility limit even at 120 mins implying a faster migration of HCO_3^- ions. Figure 4D shows the effect of AEM thickness varied from 50 to 150 μm. The transient CO_2 concentration is inversely proportional to the thickness of the AEM. Thinner membranes have sharper concentration gradients that enhances the transport from the organic side to the aqueous side.

Moreover, since the membrane is modeled as a solid electrolyte, the diffusion coefficients of the species in the membrane are relatively lower compared to the aqueous or the organic diffusion coefficients, causing slower diffusion of the ions. Therefore, thicker membranes exhibit a slower rate of CO_2 capture. The effect of feed RH is shown in Figure 4E. Since the mechanism relies on the moisture gradient to effectively capture CO_2, the higher RH implies higher water concentration on the organic side and consequently, making it easier for the HCO_3^- to convert back to CO_3^{2-} and CO_2 on the organic side, which can lead to CO_2 to bubble out of the organic side making the CO_2 capture inefficient. Therefore, a low RH is preferable for an efficient CO_2 capture by this mechanism.

3.4 CO_2 utilization flux and performance curves

As the CO_2 capture system reaches the solubility limit for CO_2 on the aqueous side, the surplus CO_2 available as a result of migration of HCO_3^- converts to gaseous CO_2 and bubbles out. To prevent this and better utilize CO_2 on the aqueous side, a CO_2 utilization flux can be established in the model to convert CO_2 to value-added products by the following equation electrochemically:

$$flux_{CO_2\,utilization} = \frac{-i_{CO_2}}{nF} \tag{8}$$

where $-i_{CO_2}$is the CO_2 utilization current density, and the negative sign indicates the removal of CO_2 from the aqueous side, n is the number of electrons transferred, and F is the Faraday's constant. Here, $n = 2$ is implemented on the aqueous side for the conversion of CO_2 to CO.

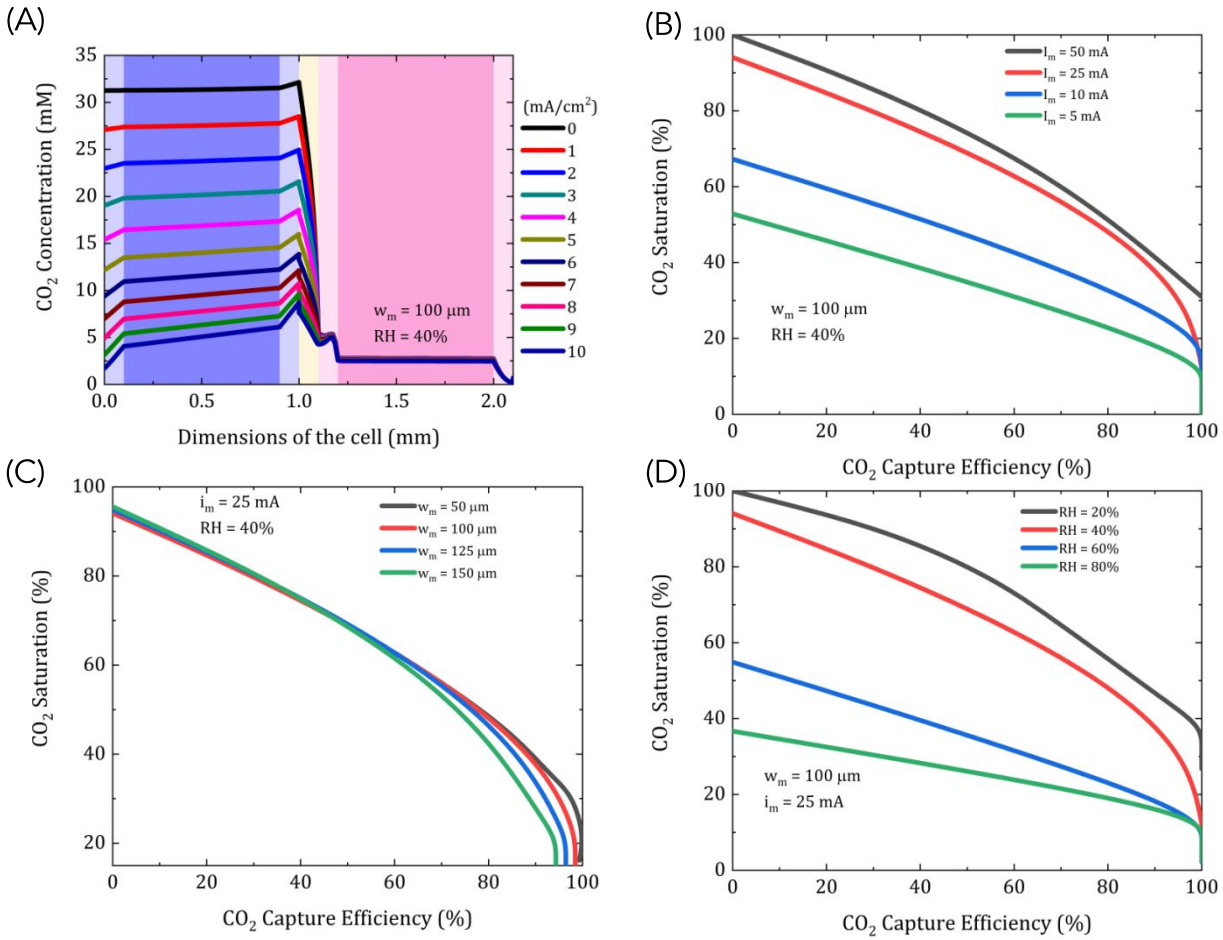

Figure 5: (A) CO_2 concentration profile at steady-state with varying CO_2 utilization current densities. Effect of (B) migration current, (C) membrane thickness, and (D) feed RH on the performance curves of the MAMG CO_2 capture process.

Figure 5A shows the effect of CO_2 utilization current density on the CO_2 concentration profile on the aqueous side. As the CO_2 utilization flux increases, the concentration of dissolved CO_2 in the aqueous side decreases and remains below its solubility limit thus, preventing the bubbling-out of CO_2.This integration of CO_2 utilization flux upgrades the system to behave as a CO_2 capture and utilization (CCU) unit, which is an efficient approach to concurrently controlling the prevalence of anthropogenic CO_2 and reducing fossil fuel consumption(44, 45). This simultaneous capture and utilization of CO_2 can realize high efficiencies only when the flux of CO_2 captured $\geq$ the flux of CO_2 utilization.(16)As discussed previously, adding auxiliary CO_2 regeneration to a discontinuous CO_2 utilization process increases its capital and operating cost and hence is a bottleneck for a successful implementation of CCU. The CO_2 capture and release mechanism of MAMG technology circumvents this challenge, and therefore, appropriate metrics are needed to evaluate the performance of this system. Here we define the performance of a MAMG CO_2 capture process by 2 key metrics- CO_2 capture efficiency and CO_2 saturation. CO_2 capture efficiency is defined as:

$$CO_2\ capture\ efficiency = \frac{CO_2\ utilization\ flux}{HCO_3^-\ crossover\ flux} \quad (9)$$

where CO_2 utilization flux is defined in eq. (8), and HCO_3^- crossover flux is the back-diffusion flux of CO_2 across the AEM into the organic side due to a large concentration difference in the concentration between the two sides. CO_2 saturation is defined as:

$$CO_2\ saturation = \frac{[CO_2]_{aqueous}}{[CO_2]_{max}} \quad (10)$$

where $[CO_2]_{aqueous}$ is the concentration of CO_2 on the aqueous side and $[CO_2]_{max}$ is the maximum concentration of CO_2 in an aqueous solution (~33mM).Using the two metrics in eq. (9) and (10), performance curves have been created to evaluate the system's performance with varying process parameters. Figure 5B-D show the effect of process parameters on the performance curves. Ideally, a square-shaped performance curve should imply 100% CO_2 saturation for any CO_2 capture efficiency. This means that a process should have no crossover of CO_2 back to the organic side for any rate of CO_2 utilization from the aqueous side. However, a non-ideal process deviates from this behavior due to slow diffusion across the AEM and the back diffusion of CO_2, HCO_3^-, and CO_3^{2-} to the organic side due to the concentration difference of the species between the organic and the aqueous sides. Figure 5B shows the effect of migration current on the performance curves. This is similar to the effect seen in Figure 4C for the change in CO_2 concentration with the migration current. The system performs better (i.e., has a larger area under the performance curve) at higher migration current densities as the flux of CO_2 in the aqueous side is larger, and there is more CO_2 available to utilize on the aqueous side. Figure 5C shows the effect of membrane width on the performance curve, which is analogous to the change in CO_2 concentration in Figure 4D. Thicker membranes are less efficient as they have a persistent back diffusion of CO_2 that prevents the system from reaching 100% capture efficiency. The effect of RH is seen in Figure 5D. As a lot of captured CO_2 on the organic side is lost due to the presence of high concentrations of water in the feed, the CO_2 saturation does not reach 100% at higher RH. Therefore, the performance of such a system is best at high migration current with thinner membranes and low RH of the CO_2 feed.

3.5 Machine learning-driven prediction of performance curves

Complex physics-based simulations like the one described in this work can be computationally expensive. Hence, synergistic incorporation of ML (46-48) with such a physics-based model can accelerate identifying the optimum operating conditions for MAMG CO_2 capture. The two ML-based models were optimized to predict the CO_2 separation efficiency based on the operating parameters such as RH, membrane thickness, migration current, and CO_2 utilization flux. NN model showed a strong correlation between the actual separation efficiency and the predicted separation efficiency. The most critical operating parameters (i.e., features) are CO_2 utilization flux, RH, and migration current. Figure 6 shows the contour of separation efficiency generated by the NN model. Details on the ML models are given in section S6 of the ESI.

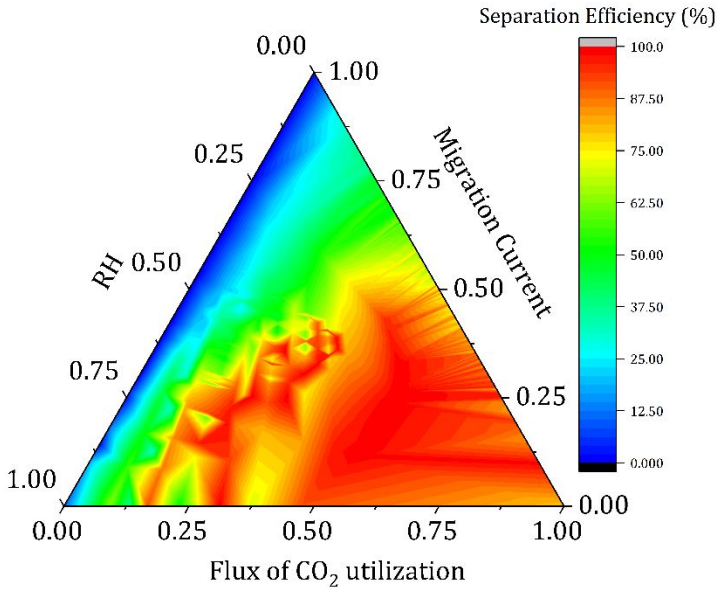

Figure 6: ML-generated ternary contour representing the dependence of CO_2 separation efficiency on migration current, RH, and the flux of CO_2 utilization using the NN model. Each of the features is defined on a normalized scale.

It can be seen from the contour that the CO_2 utilization flux has the most substantial influence on the CO_2 separation efficiency. The MAMG CO_2 capture can exhibit a CO_2 separation efficiency >90% (red zone) at high CO_2 utilization fluxes. Even though low migration current and high RH may negatively impact the CO_2 capture, if the CO_2 on the aqueous side is utilized at a high rate, there will be no back-diffusion and crossover of the HCO_3^- ions from the aqueous side to the organic side. This insight from this ML-driven approach suggests that the MAMG CO_2 capture technology is a promising candidate for integrated CO_2 capture and conversion as the efficiency of this technology relies on constant conversion (utilization) of the CO_2 on the aqueous side.

3.6 Energy consumption of MAMG CO_2 capture and techno-economic analysis

CO_2 capture efficiency and CO_2 saturation metrics are useful in comparing the MAMG CO_2 capture systems with different process parameters. However, it is equally important to compare this process with the existing state-of-the-art CO_2 capture processes. The key metrics that can be used for a more general comparison of CO_2 capture technologies across the literature are the CO_2 capture flux (mmol of $CO_2/m^2/s$) and the energy of the CO_2 capture and release process (kJ/mol of CO_2 captured). As stated above, the current system exhibits a high flux of 2.3 mmol of $CO_2/m^2/s$. The total energy consumed per mol of CO_2 captured by this system can be calculated by:

$$E_{CO_2} = \frac{P}{flux_{CO_2\ capture} \times Area} = \frac{i_m \times V}{flux_{CO_2 capture} \times Area} = 245\ kJ/mol \qquad (11)$$

where $P = i_m \times V$ is the power consumed $i_m = 75\ mA, V = 3V, flux_{CO_2capture} = 2.3\ mmol/m^2/s$, and $Area = 4\ cm^2$.

This value of energy consumption includes water electrolysis energy of at least 237/2 = 119 kJ/mol of CO_2. Therefore, the energy consumption of CO_2 capture compensated for water electrolysis is ~126 kJ/mol of CO_2, which is the energy consumption due to electric field in the electrodialysis unit.

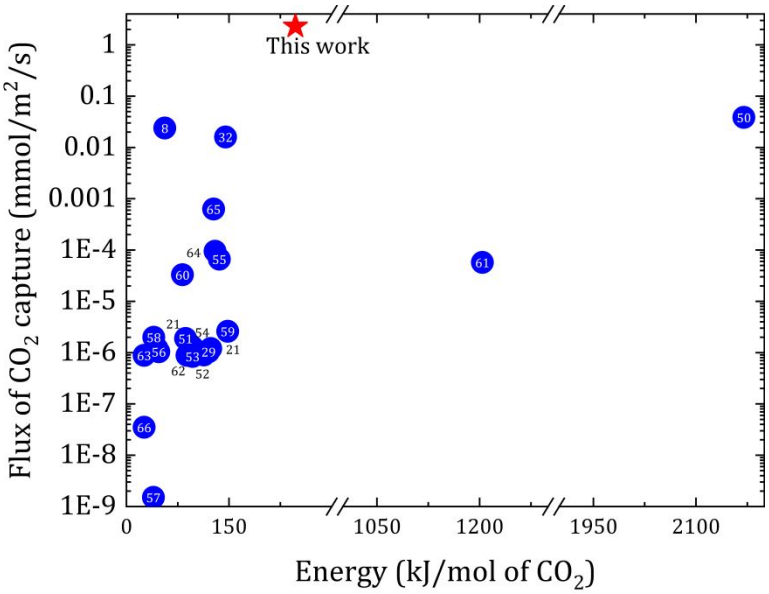

Figure 7: Comparison of flux of CO_2 capture vs. energy consumed for a CO_2 capture and release process of the MAMG CO_2 capture process with the current CO_2 capture process in the literature.(8, 21, 29, 49-66).

Figure 7 shows the comparison of the MAMG CO_2 capture process with the current state-of-the-art capture process in the recent literature using the universal metrics- the energy of CO_2 capture and release and the flux of CO_2 capture. As can be seen from the figure that the system in this work has a very high CO_2 capture flux, and due to the nature of its mechanism, there is no energy penalty for releasing the CO_2. This reduces the total energy consumption significantly to almost half of the energy consumed by the most energy-intensive but efficient CO_2 capture processes.

To achieve carbon neutrality, by 2050, 1 billion tons of CO_2 will need to be removed from the atmosphere. At current costs of $600 - $800 / ton of CO_2, the world would need to spend $600 - $800 billion / year in carbon capture. The industry needs to reach a cost of $100 - $150 / ton of CO_2 to remove government subsidies and exist as a self-sustaining business. (67) Hence, it is crucial to assess the feasibility of scaling up the MAMG CO_2 capture process as removing CO_2 to understand the likelihood of a large-scale deployment of such a technique. A brief techno-economic analysis is performed to estimate the cost of scaling up the MAMG CO_2 capture technology to capture CO_2 from a point source at a rate of 1000 ton/hr. The total cost includes the cost of the commercially available electrodialysis (ED) stacks modified to work as MAMG CO_2

capture units and the electricity cost of operation of these stacks. The details of the techno-economic analysis can be seen in section S4 of ESI. The total cost of establishing and operating the MAMG CO_2 capture technology depends on the CO_2 capture capacity. However, with the increasing availability of cheap and stable electricity, the operating cost is not a significant part of the expense, and the cost of membranes and ED stacks primarily governs the economy of scaling up this process. Membranes are consumables in this process with an average lifetime of 2-8 years (68-70). ED stacks are becoming increasingly popular due to their robust performance but are still an expensive investment costing >$200,000/stack for a capacity of processing liquids at a flow > 2000 L/hr. The area of the membrane drives the CO_2 capture rate of the MAMG process, and hence, for a larger capacity of CO_2 capture, a larger area of membranes is required. Consequently, multiple ED stacks are required to provide this area. For a fixed CO_2 capture capacity of 1000 ton CO_2/hr, the membrane area and the number of ED stacks are constant, and the total cost is dependent on the lifetime of membranes. Table 1 shows the total cost of a scaled-up MAMG process with the varying lifetime of the membranes. It can be seen that the total cost of this technology decreases with the increase in the lifetime of the membranes. For an average lifetime of 5 years, the MAMG CO_2 capture technology can capture 1000 ton/hr of CO_2 at the expense of ~$145/ton of CO_2, which meets DoE recommendations (67).

Table 1: Total cost of a scaled-up MAMG CO_2 capture process with varying membrane lifetime

Lifetime of membranes (years)	**Total cost of MAMG CO_2 capture technology ($/ton CO_2)**
1	205
2	167
5	145
8	139
10	137

4 Conclusions

In this work, we studied the water-dependent reaction of the CO_3^{2-}-HCO_3^- equilibrium under water-deprived conditions using FTIR and KF titrations, which had not been explored before in the literature. We found that the presence of water autocatalyzes the dissociation of HCO_3^- into CO_3^{2-} and CO_2, and the equilibrium constant varies with the concentration of water in a water-deprived conditions. The DFT-predicted reaction energy for HCO_3^- dissociation also corroborates these findings as it shows positive ΔG at lower concentrations of water and becomes increasingly negative at water concentrations greater than 3M. Using this information, we hypothesized that capturing CO_2 in a CO2BOL under water-deprived conditions can convert the captured CO_2 into HCO_3^- and that can be transported across an AEM to an aqueous side to convert the HCO_3^- back to CO_2, and this transport can be enhanced by applying an electric field across the membrane. Exploiting the water-dependent mechanism, we demonstrate a working prototype of MAMG CO_2 capture to realize a high CO_2 capture flux of 2.3 mmol of $CO_2/m^2/s$ from a dilute source of 10%

CO_2 and 90% N_2. A continuum model using COMSOL Multiphysics is developed to evaluate the effect of process parameters like the effect of migration current, membrane thickness, and feed RH. Determining the optimum operating conditions was accelerated by incorporating ML algorithms that accurately predicted the CO_2 separation efficiency for any given CO_2 utilization flux, migration current, and feed RH. The system's performance is evaluated by using CO_2 capture and CO_2 saturation as the metrics, and we observe that such a system would work best with high migration current, thin membranes, and lower CO_2 feed RH. The total energy consumption of this process was calculated to be 245 kJ/mol (or 126 kJ/mol with energy compensation for water electrolysis), which is lower than the efficient but energy-intensive processes in the literature due to its zero-energy penalty for the CO_2 release. Finally, a brief techno-economic analysis suggested that a scaled-up MAMG CO_2 capture technology can capture 1000 ton/hr of CO_2 at the total cost of \$145/ton CO_2. This expense is within the Department of Energy (DOE)-recommended cost/ton of CO_2 and hence, opens new avenues to further explore this technology for a sustainable scale-up for continuous CO_2 capture and release.

Acknowledgments

This material is based on the work performed in the Materials and Systems Engineering Laboratory at the University of Illinois at Chicago in collaboration with Braskem, Dr. Anh Ngo's Lab and Dr. Jindal Shah's Lab. This material is based upon work supported by the U.S. Department of Energy, Office of Science, Office of Basic Energy Sciences Direct Air Capture program under Award Number DE-SC-0022321. M.R.S. acknowledges funding support from Braskem America.

Author Contributions

Aditya Prajapati: Planned and performed CO_2 capture experiments, FTIR experiments, KF experiments, and COMSOL simulations. Analyzed the data. Wrote the first draft and edited the manuscript and ESI.

Rohan Sartape: Planned and performed the CO_2 capture experiments. Wrote the revised draft and edited the manuscript.

Tomás Rojas: Developed the theory and performed the computations. Analyzed the data. Wrote the first draft and edited the manuscript and ESI.

Naveen K. Dandu: Developed the theory and performed the computations. Analyzed the data. Wrote the first draft and edited the manuscript and ESI.

Pratik Dhakal: Developed the machine learning model. Wrote the revised draft and edited the manuscript.

Amey S. Thorat: Developed the machine learning model. Wrote the revised draft and edited the manuscript.

Jiahan Xie: Analyzed the data. Edited the manuscript. Provided critical feedback to help shape the work.

Ivan Bessa: Analyzed the data. Edited the manuscript. Provided critical feedback to help shape the work.

Miguel T. Galante: Analyzed the data. Edited the manuscript. Provided critical feedback to help shape the work.

Marcio H. S. Andrade: Analyzed the data. Edited the manuscript. Provided critical feedback to help shape the work.

Robert T. Somich: Analyzed the data. Edited the manuscript. Provided critical feedback to help shape the work.

Marcio V. Reboucas: Analyzed the data. Edited the manuscript. Provided critical feedback to help shape the work.

Gus T. Hutras: Analyzed the data. Edited the manuscript. Provided critical feedback to help shape the work.

Nathalia Diniz: Analyzed the data. Edited the manuscript. Provided critical feedback to help shape the work.

Anh T. Ngo: Developed the theory and performed the computations. Analyzed the data. Wrote the first draft and edited the manuscript and ESI.

Jindal Shah: Developed the machine learning model. Analyzed the IR data. Wrote the first draft and edited the manuscript.

Meenesh Singh: Devised the project, the main conceptual ideas, and proof outline. Worked on almost all the technical aspects. Wrote the first draft in consultation with all the co-authors.

Conflict of Interest Statement

A PCT application titled “Artificial Photosynthetic Systems for Integrated Carbon Capture and Conversion.” (UIC-2020-034) has been filed.

References

1. Goeppert, A., et al. "Air as the renewable carbon source of the future: an overview of CO_2 capture from the atmosphere." *Energy & Environmental Science* 5.7 (2012): 7833-7853.
2. Samanta, A., et al. "Post-combustion CO_2 capture using solid sorbents: a review." *Industrial & Engineering Chemistry Research* 51.4 (2012): 1438-1463.

3. Wu, X. Y., and Ghoniem. A. F. "Mixed ionic-electronic conducting (MIEC) membranes for thermochemical reduction of CO_2: A review." *Progress in Energy and Combustion Science* 74 (2019): 1-30.
4. Roy, S., Arjun C., and Peter, S. C. "Thermochemical CO_2 hydrogenation to single carbon products: scientific and technological challenges." *ACS Energy Letters* 3.8 (2018): 1938-1966.
5. Lougou, B. G., et al. "Analysis of CO_2 utilization into synthesis gas based on solar thermochemical CH_4-reforming." *Journal of Energy Chemistry* 28 (2019): 61-72.
6. Mustafa, A., et al. "Current technology development for CO_2 utilization into solar fuels and chemicals: A review." *Journal of Energy Chemistry* 49 (2020): 96-123.
7. Jones, J., Surya Prakash, G. K., and Olah G. A. "Electrochemical CO_2 reduction: recent advances and current trends." *Israel Journal of Chemistry* 54.10 (2014): 1451-1466.
8. Liu, Y., et al. "Electrochemically mediated carbon dioxide separation with quinone chemistry in salt-concentrated aqueous media." *Nature Communications* 11.1 (2020): 1-11.
9. Appel, A. M., et al. "Frontiers, opportunities, and challenges in biochemical and chemical catalysis of CO_2 fixation." *Chemical Reviews* 113.8 (2013): 6621-6658.
10. Erlach, B., Schmidt M., and Tsatsaronis, G. "Comparison of carbon capture IGCC with pre-combustion decarbonisation and with chemical-looping combustion." *Energy* 36.6 (2011): 3804-3815.
11. Theo, W. L., et al. "Review of pre-combustion capture and ionic liquid in carbon capture and storage." *Applied Energy* 183 (2016): 1633-1663.
12. Scheffknecht, G., et al. "Oxy-fuel coal combustion—A review of the current state-of-the-art." *International Journal of Greenhouse Gas Control* 5 (2011): S16-S35.
13. Suicmez, V. S. "Feasibility study for carbon capture utilization and storage (CCUS) in the Danish North Sea." *Journal of Natural Gas Science and Engineering* 68 (2019): 102924-102935.
14. Wang, M., et al. "Post-combustion CO_2 capture with chemical absorption: A state-of-the-art review." *Chemical Engineering Research and Design* 89.9 (2011): 1609-1624.
15. Leung, D. Y. C., Caramanna G., and Maroto-Valer, M. M. "An overview of current status of carbon dioxide capture and storage technologies." *Renewable and Sustainable Energy Reviews* 39 (2014): 426-443.
16. Prajapati, A., and Singh, M. R. "Assessment of artificial photosynthetic systems for integrated carbon capture and conversion." *ACS Sustainable Chemistry & Engineering* 7.6 (2019): 5993-6003.
17. Yang, S., Yu Q., and Yang S. "Development of a Full CO_2 Capture process based on the rectisol wash technology." *Industrial & Engineering Chemistry Research* 55.21 (2016): 6186-6193.
18. Bhown, A. S., and Freeman, B. C. "Analysis and status of post-combustion carbon dioxide capture technologies." *Environmental Science & Technology* 45.20 (2011): 8624-8632.
19. Lv, B., et al. "Mechanisms of CO_2 capture into monoethanolamine solution with different CO_2 loading during the absorption/desorption processes." *Environmental Science & Technology* 49.17 (2015): 10728-10735.

20. Samanta, A., et al. "Post-combustion CO_2 capture using solid sorbents: a review." *Industrial & Engineering Chemistry Research* 51.4 (2012): 1438-1463.
21. Prajapati, A., Renganathan T., and Krishnaiah K. "Kinetic studies of CO_2 capture using K_2CO_3/activated carbon in fluidized bed reactor." *Energy & Fuels* 30.12 (2016): 10758-10769.
22. Xie, K., et al. "Recent progress on fabrication methods of polymeric thin film gas separation membranes for CO_2 capture." *Journal of Membrane Science* 572 (2019): 38-60.
23. Ji, Y., et al. "High-performance CO_2 capture through polymer-based ultrathin membranes." *Advanced Functional Materials* 29.33 (2019): 1900735-1900743.
24. Li, S., et al. "Nanoporous framework "reservoir" maximizing low-molecular-weight enhancer impregnation into CO_2-philic membranes for highly-efficient CO_2 capture." *Journal of Membrane Science* 570 (2019): 278-285.
25. Ho, M. T., Allinson G. W., and Wiley D. E. "Reducing the cost of CO_2 capture from flue gases using membrane technology." *Industrial & Engineering Chemistry Research* 47.5 (2008): 1562-1568.
26. Ibrahim, M. H., et al. "CO_2 capture using hollow fiber membranes: A review of membrane wetting." *Energy & Fuels* 32.2 (2018): 963-978.
27. Cui, Z., and De Montigny, D. "Part 7: A review of CO_2 capture using hollow fiber membrane contactors." *Carbon Management* 4.1 (2013): 69-89.
28. Xiao, M., et al. "CO_2 capture with hybrid absorbents of low viscosity imidazolium-based ionic liquids and amine." *Applied Energy* 235 (2019): 311-319.
29. Wang, T., et al. "Enhanced CO_2 absorption and desorption by monoethanolamine (MEA)-based nanoparticle suspensions." *Industrial & Engineering Chemistry Research* 55.28 (2016): 7830-7838.
30. Elwell, L. C., and Grant W. S. "Technology options for capturing CO_2." *Power* 150.8 (2006): 60-65.
31. Fan, S., Wang Y., and Lang, X. "CO_2 capture in form of clathrate hydrate-problem and practice." *Proceedings of the 7th International Conference on Gas Hydrates (ICGH 2011), UK*. 2011.
32. Wang, T., Lackner, K. S., and Wright A. "Moisture swing sorbent for carbon dioxide capture from ambient air." *Environmental Science & Technology* 45.15 (2011): 6670-6675.
33. Shi, X., et al. "Kinetic analysis of an anion exchange absorbent for CO_2 capture from ambient air." *PLoS One* 12.6 (2017): e0179828.
34. Mathias P. M., et al. "Improving the regeneration of CO_2-binding organic liquids with a polarity change". *Energy & Environmental Science* 6.7 (2013):2233-2242.
35. Beck, A. D. "Density-functional thermochemistry. III. The role of exact exchange." *The Journal of Chemical Phys*ics 98.7 (1993): 5648-5652.
36. Becke, A. D. "A new mixing of Hartree–Fock and local density-functional theories." *The Journal of Chemical Physics* 98.2 (1993): 1372-1377.
37. Lee, C., Weitao Y., and Parr, R. G. "Development of the Colle-Salvetti correlation-energy formula into a functional of the electron density." *Physical Review B* 37.2 (1988): 785-789.

38. Frisch, M. J. E. A., et al. "Gaussian 09, Revision d. 01.", *Gaussian Inc., Wallingford CT* 201 (2009).
39. Tomasi, J, Mennucci B., and Cammi R.. "Quantum mechanical continuum solvation models." *Chemical Reviews* 105.8 (2005): 2999-3094.
40. Jouyban, A., and Soltanpour S. "Prediction of dielectric constants of binary solvents at various temperatures." *Journal of Chemical & Engineering Data* 55.9 (2010): 2951-2963.
41. Singh, M. R., Clark E. L., and Bell A. T. "Effects of electrolyte, catalyst, and membrane composition and operating conditions on the performance of solar-driven electrochemical reduction of carbon dioxide." *Physical Chemistry Chemical Physics* 17.29 (2015): 18924-18936.
42. Singh, M. R., et al. "Hydrolysis of electrolyte cations enhances the electrochemical reduction of CO_2 over Ag and Cu." *Journal of the American Chemical Society* 138.39 (2016): 13006-13012.
43. Jin, J., et al. "An experimental and modeling/simulation-based evaluation of the efficiency and operational performance characteristics of an integrated, membrane-free, neutral pH solar-driven water-splitting system." *Energy & Environmental Science* 7.10 (2014): 3371-3380.
44. Metz, B., et al. "IPCC special report on carbon dioxide capture and storage". *Cambridge: Cambridge University Press*, 2005.
45. Von Der Assen, N., Jung J., and Bardow A. "Life-cycle assessment of carbon dioxide capture and utilization: avoiding the pitfalls." *Energy & Environmental Science* 6.9 (2013): 2721-2734.
46. Fernandez, M., et al. "Rapid and accurate machine learning recognition of high performing metal organic frameworks for CO_2 capture." *The Journal of Chemical Physics* 5.17 (2014): 3056-3060.
47. Venkatraman, V., and Alsberg B. K. "Predicting CO_2 capture of ionic liquids using machine learning." *Journal of CO_2 Utilization* 21 (2017): 162-168.
48. Rahimi, M., et al. "Toward smart carbon capture with machine learning." *Cell Reports Physical Science* (2021): 100396-100414.
49. Wang, M., Herzog M. J., and Hatton, T. A. "CO_2 capture using electrochemically mediated amine regeneration." *Industrial & Engineering Chemistry Research* 59.15 (2020): 7087-7096.
50. Eisaman, M. D., et al. "Energy-efficient electrochemical CO_2 capture from the atmosphere." *Technical Proceedings of the 2009 Clean Technology Conference and Trade Show*. 2009.
51. Moya, C., et al. "Encapsulated Ionic Liquids for CO_2 Capture: Using 1-Butyl-methylimidazolium Acetate for Quick and Reversible CO_2 Chemical Absorption." *ChemPhysChem* 17.23 (2016): 3891-3899.
52. Uehara, Y., Karami D., and Mahinpey N. "Roles of cation and anion of amino acid anion-functionalized ionic liquids immobilized into a porous support for CO_2 capture." *Energy & Fuels* 32.4 (2018): 5345-5354.
53. Zhou, Y., et al. "Designing supported ionic liquids (ILs) within inorganic nanosheets for CO_2 capture applications." *ACS Applied Materials & Interfaces* 8.8 (2016): 5547-5555.

54. Wan, M. M., et al. "Novel CO_2-capture derived from the basic ionic liquids orientated on mesoporous materials." *ACS Applied Materials & Interfaces* 6.15 (2014): 12947-12955.
55. Zhang, W., et al. "CO_2 capture with polyamine-based protic ionic liquid functionalized mesoporous silica." *Journal of CO_2 Utilization* 34 (2019): 606-615.
56. Ren, J., et al. "Supported ionic liquid sorbents for CO_2 capture from simulated flue-gas." *Chinese Journal of Chemical Engineering* 26.11 (2018): 2377-2384.
57. Slostowski, C., et al. "CeO_2 nanopowders as solid sorbents for efficient CO_2 capture/release processes." *Journal of CO_2 Utilization* 20 (2017): 52-58.
58. Freeman, S. A., et al. "Carbon dioxide capture with concentrated, aqueous piperazine." *International Journal of Greenhouse Gas Control* 4.2 (2010): 119-124.
59. Brilman, D. W. F., and Veneman R. "Capturing atmospheric CO_2 using supported amine sorbents." *Energy Procedia* 37 (2013): 6070-6078.
60. Thompson, S. J., Soukri, M., and Lail, M. "Phosphorus dendrimer derived solid sorbents for CO_2 capture from post-combustion gas streams." *Energy & Fuels* 32.8 (2018): 8658-8667.
61. Liao, J., et al. "Highly efficient and durable metal-organic framework material derived Ca-based solid sorbents for CO_2 capture." *Chemical Engineering Journal* 372 (2019): 1028-1037.
62. Qi, G., et al. "High efficiency nanocomposite sorbents for CO_2 capture based on amine-functionalized mesoporous capsules." *Energy & Environmental Science* 4.2 (2011): 444-452.
63. Jiang, B., et al. "Development of amino acid and amino acid-complex based solid sorbents for CO_2 capture." *Applied Energy* 109 (2013): 112-118.
64. Roth, E. A., Agarwal S., and Gupta, R. K. "Nanoclay-based solid sorbents for CO_2 capture." *Energy & Fuels* 27.8 (2013): 4129-4136.
65. Plaza, M., et al. "Application of thermogravimetric analysis to the evaluation of aminated solid sorbents for CO_2 capture." *Journal of Thermal Analysis and Calorimetry* 92.2 (2008): 601-606.
66. Zhu, J., et al. "Effect of immobilization methods and the pore structure on CO_2 separation performance in silica-supported ionic liquids." *Microporous and Mesoporous Materials* 260 (2018): 190-200.
67. Zoelle, A. J., et al. “Cost and Performance Baseline for Fossil Energy Plants, Volume 1: Bituminous Coal and Natural Gas to Electricity, Revision 4.” *NETL-PUB-22011*, National Energy Technology Laboratory (NETL), Pittsburgh, PA, Morgantown, WV, and Albany, OR (United States), 2018.
68. Ghalloussi, R., et al. "Ageing of ion-exchange membranes in electrodialysis: A structural and physicochemical investigation." *Journal of Membrane Science* 436 (2013): 68-78.
69. Generous, M. M., et al. "Techno-economic assessment of electrodialysis and reverse osmosis desalination plants." *Separation and Purification Technology* 272 (2021): 118875-118896.
70. Sabatino, F., et al. "Evaluation of a direct air capture process combining wet scrubbing and bipolar membrane electrodialysis." *Industrial & Engineering Chemistry Research* 59.15 (2020): 7007-7020.